# Selection of a Pentameric Host in the Host–Guest Complexes {[{[P(μ-N*t*Bu)]$_2$(μ-NH)}$_5$]·I}$^-$[Li(thf)$_4$]$^+$ and [{[P(μ-N*t*Bu)]$_2$(μ-NH)}$_5$]·HBr·THF

**Felipe García,[a] Jonathan M. Goodman,[a] Richard A. Kowenicki,[a] Istemi Kuzu,[a] Mary McPartlin,[b] María A. Silva,[a] Lucía Riera,*[a] Anthony D. Woods,[a] and Dominic S. Wright*[a]**

**Abstract:** The structures of the host–guest complexes {[{[P(μ-N*t*Bu)]$_2$(μ-NH)}$_5$]I}$^-$·[Li(thf)$_4$]$^+$ [**2**·I{Li(thf)$_4$}] and [{[P(μ-N*t*Bu)]$_2$(μ-NH)}$_5$]·HBr·THF (**2**·HBr·THF) show that increased distortion of the framework of the pentameric macrocycle [{[P(μ-N*t*Bu)]$_2$(μ-NH)}$_5$] (**2**) occurs with the larger halide ions. Theoretical studies show that the thermodynamic stabilities of the model host–guest anions [**2**·X]$^-$ (X = Cl, Br, I) are in the order Cl$^-$ ≈ Br$^-$ > I$^-$, that is, the reverse of the templating trend observed experimentally. These studies support the view that the selection of the pentamer **2** over the tetramer [{[P(μ-N*t*Bu)]$_2$(μ-NH)}$_4$] (**1**) is kinetically controlled, a conclusion which is also consistent with the previous observation that the frameworks of **1** and **2** are not in dynamic equilibrium with each other.

**Keywords:** halides · host–guest systems · macrocycles · P heterocycles · phosphazane

## Introduction

In 1980 Scherer and co-workers reported the phosphazane [{[P(μ-N*i*Pr)]$_2$(μ-N*i*Pr)}$_2$], composed of two $P_2N_2$ rings linked together into a cyclic arrangement by bridging *i*PrN groups.[1] However, the prospect that this cyclic dimer might represent a broader range of homologous macrocycles of this type[2] was not realised until recently.[3,4] By reducing the steric demands of the linking groups we were able to obtain the cyclic tetramer [{[P(μ-N*t*Bu)]$_2$(μ-NH)}$_4$] (**1**) almost quantitatively from the condensation reaction of [{H$_2$NP(μ-N*t*Bu)}$_2$] with [{ClP(μ-N*t*Bu)}$_2$] (1:1 equivalents) in the presence of $Et_3N$ (Figure 1a).[3] A minor product of this reaction (0.5–1 % yield) is the host–guest complex [{[P(μ-N*t*Bu)]$_2$(μ-NH)}$_5$]·HCl·THF (**2**·HCl·THF), in which the Cl$^-$ ion is coordinated nearly symmetrically within the cavity of the macrocyclic pentamer [{[P(μ-N*t*Bu)$_2$]$_2$(μ-NH)}$_5$] (**2**) by five N–H···Cl hydrogen bonds (Figure 1b).[4] Since the hydrogen atom of the HCl unit in **2**·HCl·THF could not be located in the X-ray crystallographic study, and spectroscopic studies proved inconclusive, there remains some uncertainty as to the exact composition of this species, for example, whether the HCl unit is *intact* or whether the H$^+$ ion is bonded to the N or P atoms of **2**. Extensive $^{31}$P NMR spectroscopic studies support the view that a "divergent" mechanism is involved in the formation of **1** and **2**·HCl·THF in this reaction (Scheme 1), a combination of pre-organisation by the favoured *cis* conformations of the dimeric precursors [{H$_2$NP(μ-N*t*Bu)}$_2$] and [{ClP(μ-N*t*Bu)}$_2$] and templating by Cl$^-$ being responsible for cyclisation rather than polymerisation.[4] Importantly, these studies also revealed that the tetramer **1** and the pentamer **2** are not in dynamic equilibrium with each other, showing that the formation of these frameworks is the result of kinetic rather than thermodynamic control.[4] $^{31}$P spectroscopic studies of the reaction products also showed that the formation of **2** can be templated by excess halide ions in the order I$^-$ > Br$^-$ > Cl$^-$, a result which we ascribed to the apparent better size match of I$^-$ compared to Cl$^-$ for the cavity.[4]

We report here further studies of the reactions of [{H$_2$NP(μ-N*t*Bu)}$_2$] with [{ClP(μ-N*t*Bu)}$_2$] in the presence of LiX (X = Cl$^-$, Br$^-$, I$^-$) aimed primarily at the development of an efficient synthesis of the pentameric macrocycle **2**. The synthesis and structures of the new host–guest complexes **2**·HBr·THF and [**2**·I{Li(thf)$_4$}] are reported, the latter being the first viable source of the pentamer for future coordination studies. Molecular orbital (MO) calculations on the for-

[a] F. García, Dr. J. M. Goodman, R. A. Kowenicki, I. Kuzu, Dr. M. A. Silva, Dr. L. Riera, Dr. A. D. Woods, Dr. D. S. Wright
Chemistry Department, University of Cambridge
Lensfield Road, Cambridge CB2 1EW (UK)
Fax: (+44) 1223-336-362
E-mail: lr252@hermes.cam.ac.uk
dsw1000@cus.cam.ac.uk.

[b] Dr. M. McPartlin
Department of Health and Biological Science
London Metropolitan University, London N7 8DB (UK)



DOI: 10.1002/chem.200400320

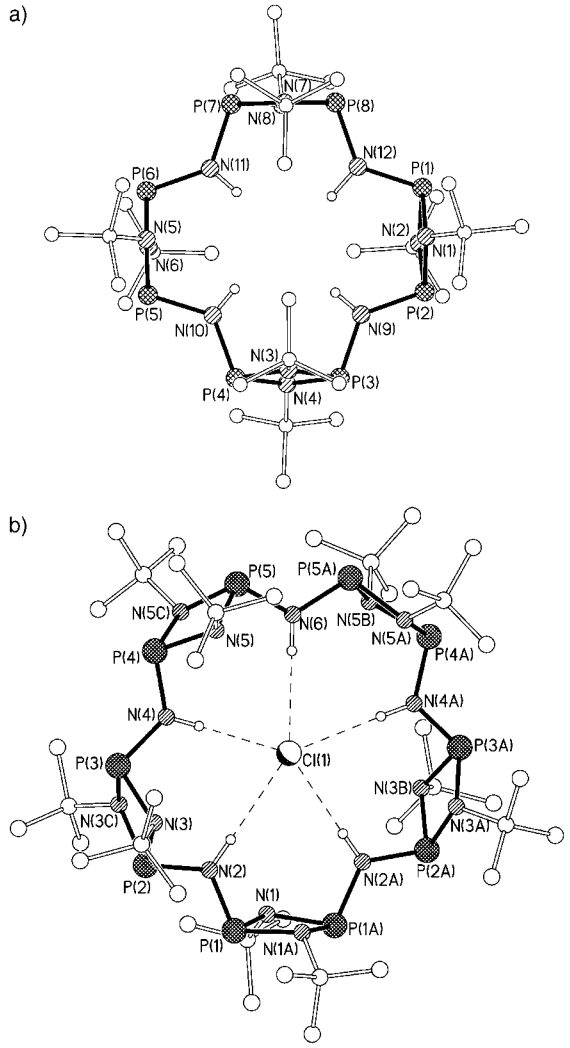


Figure 1. Structures of a) the tetramer **1** and b) the host–guest complex **2**·HCl·THF (the lattice-bound THF molecule is not shown).

mation of the anions $[\mathbf{2}\cdot X]^-$ provide further evidence that the selection of the pentamer is kinetically controlled.

## Results and Discussion

**Synthetic and structural studies:** Although previous in situ $^{31}$P NMR spectroscopic studies had shown the pentamer **2** is formed in the absence of the tetramer **1** in the 1:1 stoichiometric reaction of $[\{H_2NP(\mu\text{-}N\mathit{t}Bu)\}_2]$ with $[\{ClP(\mu\text{-}N\mathit{t}Bu)\}_2]$ in the presence of excess LiI in THF, preparative-scale reactions result in a complicated mixture of solid products and **2** could not be obtained in good yield or in pure form using this procedure. However, we noted earlier that the formation of the pentameric arrangement can only be explained by a competing ring-closing step involving $[\{NH_2P(\mu\text{-}N\mathit{t}Bu)\}_2]$, since a consecutive head-to-tail reaction of the components could only produce rings with an even number of constituents (such as the tetramer **1**; Scheme 1).[4] With this in mind, we undertook the 3:2 reactions of $[\{NH_2P(\mu\text{-}N\mathit{t}Bu)\}_2]$ with $[\{ClP(\mu\text{-}N\mathit{t}Bu)\}_2]$ in the presence of LiX (X = $Cl^-$, $Br^-$, $I^-$) (1:6 equiv, respectively). Even after prolonged reflux, the presence of LiCl or LiBr in these reactions resulted only in a similar mixture of apparent chain products, with little of **1** or **2** being formed. For example, the in situ $^{31}$P NMR spectrum of the reaction mixture in the presence of LiBr shows a collection of well-resolved, overlapping multiplets in the region $\delta = 94$–$134$ ppm, with resonances at about $\delta = 115.0$ ppm and about $\delta = 130.0$ ppm being found for **2**·HBr and **1**, respectively. In this case, extraction with *n*-pentane followed by crystallisation of the crude solid from *n*-pentane/THF gave a low yield of the crystalline THF solvate **2**·HBr·THF (ca. 1–2%). Despite repeated attempts, we were unable to obtain pure samples of **2**·HBr free from contamination with variable amounts of apparent chain prod-

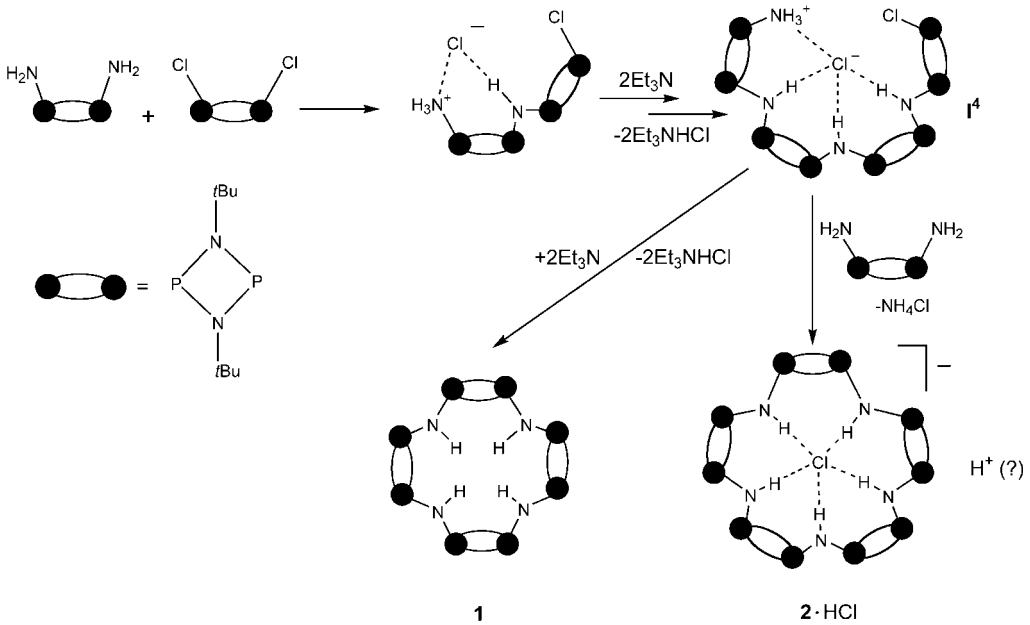


Scheme 1. A possible "divergent" mechanism for the formation of **1** and **2**·HCl·THF.

  

ucts and consequently we were unable to obtain satisfactory elemental analysis on the complex. The impurities present in samples of **2**·HBr also precluded more extensive $^{1}H$ and $^{31}P$ NMR spectroscopic investigations. However, we were able obtain single crystals of **2**·HBr suitable for an X-ray diffraction study and, hence, characterise the complex in the solid state. It can be noted that all of the crystals obtained on separate samples of the complex could be identified as **2**·HBr by unit cell analysis. In addition, in previous studies the presence of **2**·HBr in the crude reaction mixture had been inferred by positive-ion electrospray mass spectroscopy, which showed the presence of $[\mathbf{2}\cdot H_2Br]^+$.[4] Interestingly, despite protonation of one of the P centres of the pentameric framework in **2**·HBr (shown by later X-ray analysis to be of the form $[\mathbf{2}\cdot H]^+Br^-$) only a singlet is observed in the $^{31}P$ NMR spectrum of this complex in solution at room temperature. This suggests that either intermolecular proton exchange is occurring (e.g., involving solvent) or a fluxional process in which the $H^+$ ion is processing around the pentamer, being passed from one P to the next P centre in the ring unit. This suggested mechanism is in contrast to the results obtained by Niecke and co-workers on a P-protonated diphosph(III)azane dimer in which a static structure is shown by $^{31}P$ NMR spectroscopic studies.[5]

A similar mixture of products to that formed in the LiBr reaction is also generated in the room-temperature reaction of $[\{NH_2P(\mu\text{-}NtBu)\}_2]$ with $[\{ClP(\mu\text{-}NtBu)\}_2]$ in the presence of LiI. However, after reflux the in situ $^{31}P$ NMR spectrum of the reaction mixture shows only the presence of $[\mathbf{2}\cdot I\{Li(thf)_4\}]$ ($\delta = 115.2$ ppm) and traces of **1**. Crystalline **2**·I{Li(thf)$_4$} is isolated in 44% yield after extraction with *n*-pentane and crystallisation from *n*-pentane/THF. The $^{31}P$ NMR spectrum of isolated **2**·I{Li(thf)$_4$} at room temperature shows only a singlet at $\delta = 115.2$ ppm due to the *intact* complex, irrespective of the concentration. This assignment is supported by the fact that the spectrum does not change on addition of LiI (thus, this resonance cannot result from dissociation into **2** and LiI). The $\mathbf{2}\cdot I^-$ ion is also observed in the negative-ion electrospray mass spectrum of **2**·I{Li(thf)$_4$} ($m/z = 1222.3$).

The low-temperature X-ray structures of **2**·I{Li(thf)$_4$} and **2**·HBr·THF were obtained. Details of the data collections and refinements of **2**·I{Li(thf)$_4$} and **2**·HBr can be found in Table 1, while key bond lengths and angles for these compounds are mentioned in the text and in the captions to Figures 2 and 3.

The solid-state structure of **2**·HBr·THF (Figure 2) consists of a host–guest complex of the pentamer **2** with HBr, together with a lattice-bound THF molecule. The crystallographic analysis of **2**·HBr·THF suggests strongly that the complex consists of a protonated $[\mathbf{2}\cdot H]^+$ ion which coordinates a $Br^-$ ion within the cavity. This conclusion is not only supported by the direct location of the H-atom bonded to P(1) but by a more detailed analysis of the variation in the bond lengths and angles within the macrocyclic framework. As expected on the basis of the positive charge carried by P(1)(-H), there is a noticeable shortening of the associated P-μ-N(-H) (P(1)–N(15) 1.614(5) Å) and P-μ-N(*t*Bu) (P(1)–N(1) 1.651(5), P(1)–N(2) 1.633(5) Å) bond lengths in the vi-

Table 1. Details of the structure refinements and data collections on **2**·HBr and **2**·I{Li(thf)$_4$}.

| Compound | **2**·HBr·THF | **2**·I{Li(thf)$_4$} |
|---|---|---|
| empirical formula | $C_{44}H_{104}BrN_{15}OP_{10}$ | $C_{56}H_{127}ILiN_{15}O_4P_{10}$ |
| FW | 1249.03 | 1518.27 |
| $T$ [K] | 180(2) | 180(2) |
| crystal system | orthorhombic | monoclinic |
| $\lambda$ [Å] | 0.71073 | 0.71073 |
| space group | $P2(1)2(1)2(1)$ | $P2(1)/c$ |
| $a$ [Å] | 10.1489(2) | 21.417(4) |
| $b$ [Å] | 25.1105(5) | 13.359(3) |
| $c$ [Å] | 27.8804(5) | 29.692(6) |
| $\beta$ [°] | — | 99.98(3) |
| $V$ [Å$^3$] | 7105.2(2) | 8366(3) |
| $Z$ | 4 | 4 |
| $\rho_{calcd}$ [Mg m$^{-3}$] | 1.168 | 1.205 |
| reflections collected | 45672 | 29456 |
| independent reflections ($R_{int}$) | 12487 (0.088) | 11041 (0.077) |
| $R1$, $wR2$ [$I > 2\sigma(I)$] | 0.063, 0.150 | 0.060, 0.121 |
| $R1$, $wR2$ (all data) | 0.100, 0.168 | 0.112, 0.144 |

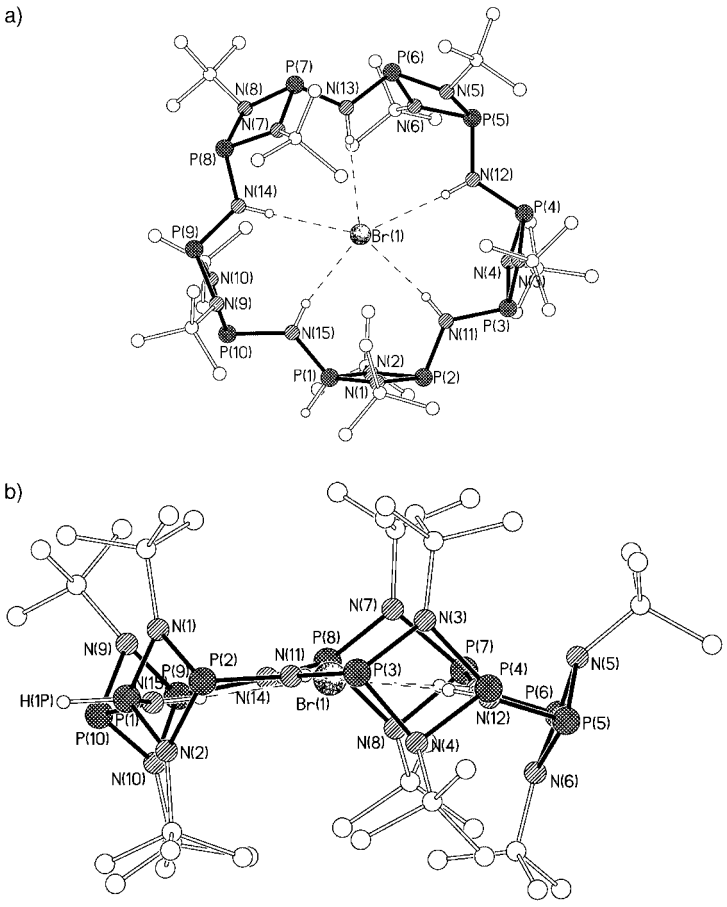


Figure 2. a) Structure of **2**·HBr·THF. Hydrogen atoms (except those attached to N and P) and the disordered THF molecule in the lattice have been omitted for clarity. b) A view parallel to the macrocyclic plane of **2**·HBr·THF, showing the tilting of the P(5)-N(5)-P(6)-N(6) ring unit. Selected bond lengths [Å] and angles [°]: P–(μ-N*t*Bu) range 1.633(5)–1.758(5), P–(μ-NH) range 1.614(5)–1.763(5), P···P in $P_2N_2$ rings range 2.557(2)–2.606(2) (mean 2.60), X···N(11–15)$_{centroid}$ 0.22; P-μ-N(*t*Bu)-P 96.9(3)–99.0(3) (mean 98.0), N(*t*Bu)-P–N(*t*Bu) 79.1(2)–85.8(2) (mean 81.8), P-μ-N(H)-P 122.0(3)–129.0(3) (mean 123.8), N–H···Br(1) range 2.41–2.62 [N···Br(1) range 3.275(5)–3.496(5), N–H···Br(1) 167–178].

cinity of P(1) compared to the other P–N bonds within **2**·HBr (range P-μ-N(-H) 1.656(5)–1.763(5), range P-μ-N(*t*Bu) 1.707(5)–1.758(5) Å). In addition, the N-P-N angles about P(1) all show a significant expansion compared to the other P centres of the complex, consistent with the removal of lone-pair/bonding pair repulsion upon protonation of P(1). This is seen in particular in the exocyclic N(15)-P(1)-N(1) and N(15)-P(1)-N(2) angles (116.7(3)° and 119.6(3)°, respectively), which are at least about 12° greater than the other exocyclic N-P-N angles for the neutral P centres in **2**·HBr·THF (range 102.7(2)–107.7(3)°). The endocyclic N(1)-P(1)-N(2) angle (85.8(2)°) is also the largest such angle found within the $P_2N_2$ ring units of the complex (range 79.1(2)–82.5(2)° for the other endocyclic N-P-N angles). The protonation of P(1) appears also to be responsible for the expansion of the P(1)-N(15)-P(10) angle (129.0(3)°) compared to the other P-μ-NH-P angles (range 122.0(3)–123.7(3)°). As noted previously, owing to disorder and to the high crystallographic symmetry of the structurally characterised THF solvate **2**·HCl·THF we had been unable to locate the $H^+$ cation of the HCl unit. There is therefore some uncertainty as to the precise composition of this compound, for example, whether an *intact* HCl unit is present or whether the N or P atoms of **2** are protonated. While the structure of **2**·HBr·THF may suggest that a similar formulation is appropriate for **2**·HCl·THF (i.e., $[\mathbf{2}\cdot H]^+Cl^-$) there remains some uncertainty. In particular, in the solid-state structure of **2**·HCl·THF, a distinctive pattern of bond lengths and angles which might suggest protonation at a P centre is not observed, with the all the P–N bond lengths being in the range 1.685(4)–1.753(3) Å and with the P-μ-NH-P angles being in the range 120.9(3)–121.4(4)°. It should be noted, however, that the hydrogen-atom position and its effect on the pentameric framework would be averaged over at least two of the P centres of the backbone, since only five of the ten P centres are crystallographically independent (see Figure 1b). The difficulty in locating such a potential hydrogen atom is exacerbated by the presence of a highly disordered THF components on either side of the cavity of **2**·HCl·THF.[4] In contrast, in **2**·HBr·THF the disordered THF molecule in the lattice is remote from the macrocyclic unit.

Apparently as a consequence of the coordination of the larger $Br^-$ ion within **2**·HBr·THF, the pentameric framework in this complex is significantly more distorted than in the HCl counterpart. In **2**·HCl·THF, the fifteen P and N atoms forming the $(P\cdots P\text{-}N)_5$ backbone of the pentamer and the $Cl^-$ ion reside almost within a plane, with the $Cl^-$ being coordinated symmetrically by all five N-H protons (H···Cl 2.52(1)–2.56(1) Å; N–H···Cl 175(5)–180(5)°).[4] In **2**·HBr·THF, the $Br^-$ ion is located about 0.22 Å above the centroid of the five N(-H) atoms. Although the anion is H-bonded to all five N-H protons of the macrocyclic pentamer,[6] the H···Br distances fall over a large range (2.41–2.62 Å). Interestingly, the shortest of these interactions is made with N(15)-H (2.41 Å), that is, the most acidic N-H proton which is adjacent to the cationic P(1)(-H) centre. Eight of the P centres and all five of the bridging N(-H) atoms in **2**·HBr are coplanar (to within 0.21 Å), with the mean planes of the four associated $P_2N_2$ ring constituents being tilted with respect to this plane by 0.2–14.5°. The remaining $P_2N_2$ ring unit {P(5)N(5)P(6)N(6)} shows the most marked distortion. This ring unit pivots about N(12) and N(13), tilting this ring by 29.8° out of the major plane of the macrocycle (Figure 2b). This conformation contrasts with that found in **2**·HCl·THF in which all five of the $P_2N_2$ ring units are perpendicular to the $[(P\cdots P)N]_5$ plane.[4]

Despite the fact that the pentameric unit of **2**·I{Li(thf)$_4$} is not protonated, the overall structural features of this complex, which consists of a $[\mathbf{2}\cdot I]^-$ ion (Figure 3) and a $[Li(thf)_4]^+$ ion, appear to be related to those found in **2**·HBr, particularly in respect to the nature of the distortion of the macrocyclic unit and the non-planar coordination of the $I^-$ ion. The $I^-$ ion of the **2**·$I^-$ anion in **2**·I{Li(thf)$_4$} is situated 1.36 Å above the centroid of the five N(-H) centres of the macrocyclic ring. Although the N–H···I H-bonds (N–H···I 2.78–2.91 Å) are all within the range of values estimated for H···I hydrogen bonds (H···I 3.15–3.57 Å),[6] two of these interactions appear to be stronger (N(11,12)–H···I 172–177°) than the remaining three (N(13,14,15)–H···I 158–

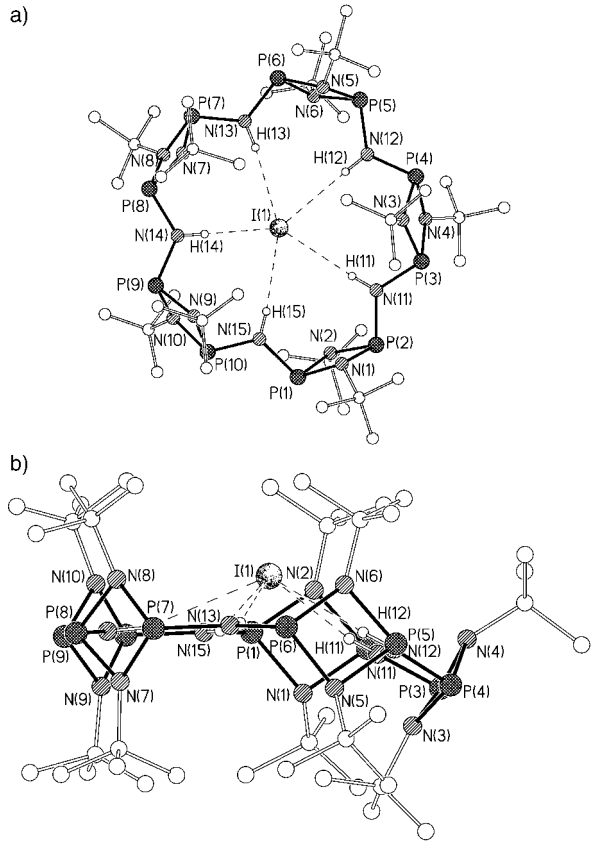


Figure 3. a) Structure of the anion **2**·$I^-$. The Li(thf)$_4^+$ ion and hydrogen atoms (except those attached to N) and have been omitted for clarity. b) A view parallel to the macrocyclic plane of the **2**·$I^-$ ion, showing the tilting of the P(3)-N(3)-P(4)-N(4) ring unit. Selected bond lengths [Å] and angles [°]: P–(μ-N*t*Bu) range 1.711(6)–1.745(5), P–(μ-NH) range 1.685(5)–1.730(6), P···P in $P_2N_2$ rings range 2.607(3)–2.619(3) (mean 2.61), $X\cdots N(11\text{–}15)_{centroid}$ 1.36; P-μ-N(*t*Bu)-P 96.8(3)–99.5(3) (mean 98.4), N(*t*Bu)-P–N(*t*Bu) 80.1(3)–82.2(2) (mean 81.1), P-μ-N(H)-P 121.7(3)–123.0(5) (mean 122.6), N–H···I(1) range 2.78–2.91 [N···I(1) range 3.690(5)–3.743(5), N–H···I(1) 158–177].

  

163°). The presence of two sets of (stronger and weaker) N–H···I bonds provides an explanation for the observation of two N-H stretching bands in the IR spectrum of **2**·I{Li(thf)$_4$} (3144 and 3104 cm$^{-1}$). The distortion of the macrocyclic unit and the asymmetrical coordination of the I$^-$ ion are related. Eight of the P centres and all five bridging N(-H) atoms of the pentameric unit of the **2**·I$^-$ ion are coplanar (to within 0.21 Å), with the mean planes of the four associated $P_2N_2$ constituents being almost perpendicular to this plane (within 7.7°). The remaining ring unit {P(3)N(3)P(4)N(4)} pivots about N(11) and N(12), tilting this ring from perpendicular by 29.1° to the major macrocyclic plane (Figure 3b; this distortion results in the N(11)-H(11) and N(12)-H(12) vectors pointing more directly at the I$^-$ ion than the other N–H atoms (thus optimising the two strongest N–H···I hydrogen bonds observed). The resulting displacement of the *t*Bu group bonded to N(3) towards the lower face of the cavity (away from the anion) presumably precludes the similar distortion of the other $P_2N_2$ ring units and the formation of stronger hydrogen bonds involving the remaining three N-H groups. The conformations of the macrocyclic units found in **2**·HBr·THF and **2**·I{Li(thf)$_4$} are broadly similar to each other, despite the accommodation of the different halide ions within the pentameric units.

**MO calculations:** Ab initio calculations of the uncoordinated pentamer **2** and the host–guest complexes **2**·X$^-$ (X = Cl$^-$, Br$^-$, I$^-$) at the restricted Hartree–Fock (RHF) level of theory with the 3–21G basis sets[7] were undertaken using various imposed symmetries.[8] Density functional theory (DFT) methods at the B3LYP/6–31G** level[9] were also employed for **2**·Cl$^-$ and **2**·Br$^-$. Interestingly, the geometry optimisations of the free pentamer **2** in $C_{5v}$ and $C_s$ symmetry (Figure 4a and 4b, respectively) reveal that the distorted $C_s$ structure is preferred to the planar $C_{5v}$ structure by 12.62 kcal mol$^{-1}$. The geometry optimisations of **2**·Cl$^-$ and **2**·Br$^-$ in which the (P···P–N)$_5$ backbone of **2** is constrained to be planar ($D_{5h}$ and $C_{5v}$ symmetry) show that the preferred arrangements are those where the X$^-$ ions reside within the cavity of **2**, with the most stable structure of **2**·Cl$^-$ being very similar to that of **2**·HCl·THF in the solid state (Figure 5a).[4] However, for **2**·I$^-$ the optimised $C_{5v}$ structure shows the I$^-$ ion displaced 1.99 Å above the centroid of **2** and it is favoured by 8.8 kcal mol$^{-1}$ over the symmetrical

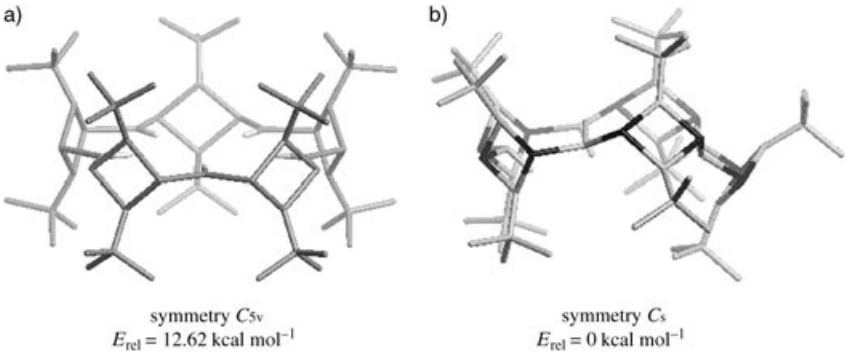


Figure 4. HF/3-21G-optimised geometries for the ligand with $C_{5v}$ and $C_S$ symmetries. Relative energies in kcal mol$^{-1}$.

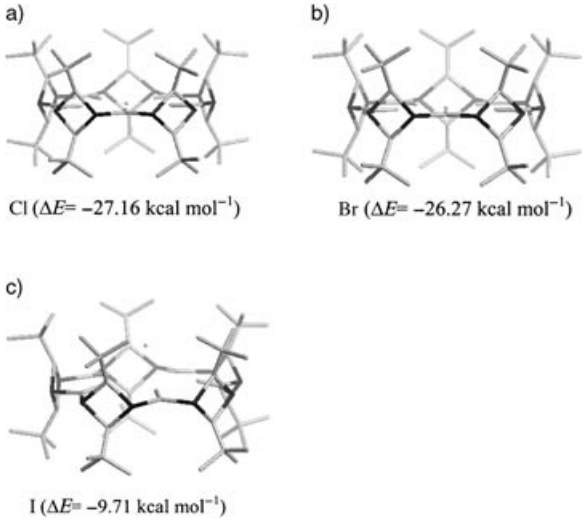


Figure 5. HF/3–21G-optimised geometries for **2**·X$^-$ (X = Cl$^-$, Br$^-$, I$^-$) with $C_{5v}$ symmetry. Reaction energies (with respect to the most stable $C_s$ structure for **2**) for **2** + X$^-$ → **2**·X$^-$, in parentheses.

($D_{5h}$) coordination of the ion within the cavity (Figure 5c). A similar structural trend is found for lower symmetry $C_s$ models, that is, for **2**·Cl$^-$ and **2**·Br$^-$ the halide ions prefer to be located essentially within the cavity (Figure 6a and 6b, respectively), whereas (similarly to the experimental structure) the I$^-$ ion of **2**·I$^-$ is displaced above the mean plane of the N(-H) groups by 1.86 Å (Figure 6c). Most significantly, for all the symmetries investigated the reaction energies ($\Delta E$) for **2** + X$^-$ → **2**·X$^-$ are in the order Cl$^-$ ≈ Br$^-$ > I$^-$. In the case of the most stable $C_s$ models investigated, ΔE for **2**·Cl$^-$ (−46.8 kcal mol$^{-1}$) and **2**·Br$^-$ (−43.1 kcal mol$^{-1}$) are about twice that for **2**·I$^-$ (−20.6 kcal mol$^{-1}$).

## Conclusion

It was already clear from our previous studies that halide ions are acting as kinetic templates in this system,[10] since the alternative products (the tetramer **1** and pentamer **2**, see Scheme 1) are not in dynamic equilibrium with each other under the reaction conditions.[4] The theoretical results show that, in addition, the templating of **2** by LiI observed experimentally is not due to the thermodynamic preference of the pentamer for I$^-$ ions. The most plausible explanation for the observed order of templating I$^-$ > Br$^-$ > Cl$^-$ is the effect of the I$^-$ ion on the framework of the pivotal intermediate **I**$^4$ (Scheme 2) and on the rates of the subsequent reactions producing **1** and **2**·X$^-$. In particular, by holding the -NH$_2$ and -Cl termini furthest apart the rate of **I**$^4$ → **1** will be retarded to the greatest extent by I$^-$ (so-

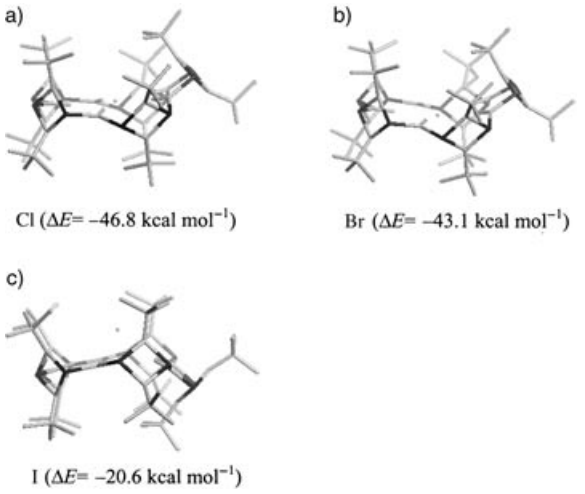


Figure 6. HF/3-21G-optimised geometries for **2**·X$^-$ (X = Cl$^-$, Br$^-$, I$^-$) with $C_s$ symmetry. Reaction energies (with respect to the most stable $C_s$ structure for **2**) for **2** + X$^-$ → **2**·X$^-$, in parentheses.

called *negative templating*[11]). It is also possible that optimum separation of these groups for reaction with [{$H_2$NP(μ-N*t*Bu)}$_2$] is also provided by I$^-$, increasing the rate of **I**$^4$ → **2** (*positive templating*[11]). An analogous situation has been demonstrated in the selection of a cyclic porphyrin tetramer (as opposed to the cyclic porphyrin dimer) from a linear porphyrin dimer, using a tetradentate template.[12] The fact that **1** is generated almost exclusively at −78 ± 25 °C in the absence of LiI in THF (in the 1:1 stoichiometric reaction),[3] but that **2** is generated almost exclusively in the presence of LiI at reflux in THF (in the 2:3 stoichiometric reaction) provides qualitative support for the view that the major effect of I$^-$ is as a negative template, that is, resulting in a drastic reduction in the rate of **I**$^4$ → **1** rather than an increase in **I**$^4$ → **2**. Unfortunately, although experimental determination of the kinetics of the reactions producing **1** (i.e., the rate constant for **I**$^4$ → **1**) and **2**·X$^-$ (i.e., the rate constant for **I**$^4$ → **2**·X$^-$) would provide the ultimate proof of this hypothesis, there is no amenable spectroscopic method available. In particular, the use of $^{31}$P NMR spectroscopy is precluded by the high temperature at which **2**·I$^-$ is formed and by the complicated mixture of chain intermediates present in the reaction mixture (which occur in the region of the resonances for **1** and **2**·X$^-$). It should be noted that the acidity of HX could also have a further effect on the selection of the tetrameric or pentameric frameworks in these reactions that has not been considered in the current study.

## Experimental Section

**General**: Compounds **2**·HBr and **2**·I{Li(thf)$_4$} are only moderately air- and moisture sensitive. They were prepared under dry, $O_2$-free $N_2$ on a vacuum line. *t*BuNH$_2$ was distilled over $CaH_2$ and stored under $N_2$ over molecular sieve (13X). $PCl_3$ was distilled and stored under $N_2$. THF and toluene were dried by distillation over sodium/benzophenone prior to the reactions. [{ClP(μ-N*t*Bu)}$_2$] was obtained from the 3:1 reaction of *t*BuNH$_2$ with $PCl_3$, respectively, in THF.[13] [{$NH_2$P(μ-N*t*Bu)}$_2$] was prepared by the reaction of [{ClP(μ-N*t*Bu)}$_2$] with a saturated $NH_3$/THF solution.[3,4] The compounds **2**·HBr·THF and **2**·I{Li(thf)$_4$} were isolated and characterised with the aid of an $N_2$-filled glove box fitted with a Belle Technology $O_2$ and $H_2O$ internal recirculation system. Melting points were determined by using a conventional apparatus and sealing samples in capillaries under $N_2$. IR spectra were recorded as Nujol mulls using NaCl plates and were run on a Perkin-Elmer Paragon 1000 FTIR spectrophotometer. Elemental analyses were performed by first sealing the samples under argon in air-tight aluminium boats (1–2 mg) and C, H and N content was analysed by using an Exeter Analytical CE-440. P analysis was obtained by using spectrophotometric means. $^1$H, $^{31}$P NMR spectra were recorded on a Bruker ATM DRX500 spectrometer, in dry deuterated [D$_8$]toluene (using the solvent resonances as the internal reference standard for $^1$H NMR and 85% $H_3PO_4$/$D_2O$ as the external standard for $^{31}$P NMR spectra). In situ $^{31}$P NMR spectroscopic studies on reaction mixtures in non-deuterated solvents were recorded using an internal [D$_6$]acetone capillary to obtain a lock.

**Synthesis of 2·HBr·THF**: $Et_3N$ (0.7 mL, excess) was added to a mixture of [{$NH_2$P(μ-N*t*Bu)}$_2$] (0.855 g, 3.75 mmol) and LiBr (1.30 g, excess 15 mmol) in THF (40 mL) at −78 °C. A solution of [{ClP(μ-N*t*Bu)}$_2$] (0.688 g, 2.5 mmol) in THF (40 mL) was then added dropwise. The mixture was stirred (2 hrs) then allowed to warm to room temperature and brought to reflux (14 h). The solvent was removed under vacuum and the resulting white residue was heated to 50 °C under vacuum (1 h, $10^{-1}$ atm) to remove residual solvent. The residue was extracted with *n*-pentane (60 mL) and filtered through Celite (P3). Gradual evaporation of the solvent under vacuum led to the precipitation of a white solid. The solid was then dissolved by the addition of THF (ca. 1 ml) and heating. Storage (−5 °C, 24 h) afforded colourless crystals of **2**·HBr (ca. 1–2%). $^{31}$P NMR spectroscopy of the crystalline material showed that apparent chain products were present with overlapping multiplets in the region $\delta$ = 94–134, and with resonances at about $\delta$ = 115.0 ppm (**2**·HBr) (ca. 60% of product estimated by integration) and about $\delta$ = 130.0 ppm (**1**) (ca. 10%). The amount of chain material varies from batch to batch but is typically 10–30% of the solid isolated after crystallisation. Typical elemental analysis calcd (%) for **2**·HBr·THF: C 40.8, H 8.2, N 17.8; found: C 41.1, H 7.9, N 15.4.

**Synthesis of 2·I{Li(thf)$_4$}**: $Et_3N$ (1.4 mL, excess) was added to a mixture of [{$NH_2$P(μ-N*t*Bu)}$_2$] (2.30 g, 7.5 mmol) and LiI (2.00 g, excess 15.0 mmol) in THF (60 mL) at −78 °C. A solution of [{ClP(μ-N*t*Bu)}$_2$] (1.38 g, 5 mmol) in THF (60 mL) was then added dropwise. The mixture

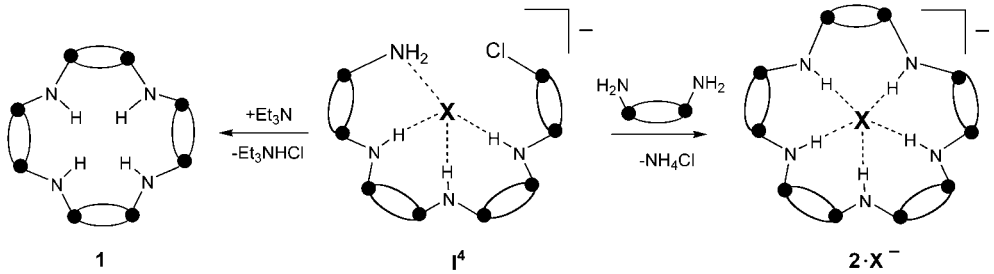


Scheme 2. The effect of the X$^-$ ion on the framework of the intermediate **I**$^4$ and the subsequent reactions to give **1** and **2**–**X**$^-$.

  

was stirred (2 h) then allowed to warm to room temperature and brought to reflux (4 h). The solvent was removed under vacuum and the resulting white residue was heated to 50 °C under vacuum (1 h, $10^{-1}$ atm) to remove residual solvent. The residue was extracted with *n*-pentane (100 mL) and filtered through Celite (P3). Gradual evaporation of the solvent under vacuum led to the precipitation of a white solid. Evaporation of the solvent was continued well past the point of precipitation. The solid was then dissolved by the addition of THF (ca. 2 mL) and heating. Storage (−5 °C, 24 h) afforded colourless crystals of **2**·I{Li(thf)$_4$}. Yield 0.84 g (44 %). M.p. 187 °C. IR (Nujol, NaCl): $\tilde{\nu}$ = 3144(w, sh), 3104(w) (N−H str.), other bands at 1261(s), 1212(s), 1157(w), 1089(m, br), 1040(s), 975(w, sh), 890(w), 802(vs) cm$^{-1}$; $^1$H NMR (500.203 MHz, [D$_8$]toluene, +25 °C): $\delta$ = 4.54 (s, 5H; N−H), 3.66 (m, 16H; -CH$_2$- THF), 1.63 (m, 4H; -CH$_2$−O THF), 1.48 ppm (s, 90H; *t*Bu); $^{31}$P NMR (202.484 MHz, [D$_8$]toluene, +25 °C, rel. 85 % $H_3PO_4$/$D_2O$): $\delta$ = 115.2 ppm (s, *intact* **2**·Li{I(thf)$_4$}); ES-MS (negative ion): *m*/*z*: 1350.4 (**2**·I$_2$H$^-$), 1222.3 (**2**·I$^-$); elemental analysis calcd (%) for **2**·Li{I(thf)$_4$}: C 44.3, H 8.4, N 13.8, P 20.4; found: C 42.6, H 8.3, N 13.8, P 19.7.

**X-ray structures of 2·HBr·THF and 2·I{Li(thf)$_4$}**: Crystals were mounted directly from solution under argon using an inert oil which protects them from atmospheric oxygen and moisture. X-ray intensity data were collected by using a Nonius Kappa CCD diffractometer. Details of the data collections and structural refinements are given in Table 1. The structures were solved by direct methods and refined by full-matrix least-squares on $F^2$.[13] The N-H and P-H protons were directly located in **2**·HBr·THF, but the structure was refined with the N−H protons in idealised positions. Two of the *t*Bu groups (attached to N(6) and N(7)) exhibited rotational disorder over two sites. The lattice-bound THF molecule was also disordered over two sites. In **2**·I{Li(thf)$_4$} the N-H protons were directly located but the structure was refined with them in idealised positions. Four of the *t*Bu groups (attached to N(3), N(8), N(9) and N(10)) exhibited rotational disorder over two sites. In both compounds all other H atoms were included in idealised positions. CCDC-230418 (**2**·HBr·THF) and CCDC-235096 (**2**·I{Li(thf)$_4$}) contain the supplementary crystallographic data for this paper. These data can be obtained free of charge via www.ccdc.cam.ac.uk/conts/retrieving.html (or from the Cambridge Crystallographic Data Centre, 12, Union Road, Cambridge CB21EZ, UK; fax: (+44) 1223-336-033; or deposit@ccdc.cam.ac.uk).

**MO calculations**: Geometry optimisation calculations were initially carried out at the semi-empirical level AM1. Although qualitatively similar results were obtained for both geometries and energies, compared to the ab initio calculations, geometries predicted by the latter gave a significant closer match to the X-ray structures. Geometry optimisations for **2**·Cl$^-$ and **2**Br$^-$ were also carried out using DFT methods at the B3LYP/6-31G** level of theory. The results of these higher level calculations correlate very closely to the ab initio level and support the results obtained at the HF/3-21G level. Frequency calculations for these large molecules at the HF/3-21G level were of prohibited computational expense and could not be performed. However, the change in energy at the HF/3–21G level with the displacement of the X$^-$ ions in **2**·X$^-$ along the $C_{5v}$ axis was calculated. The energy profile shows that the energy rises in the direction of the $C_{5v}$ axis for all the complexes. This suggests that they represent a minimum energy position under the given symmetry constraints imposed on the structures. In addition, AM1 frequency calculations were carried out and no negative modes were found, except those associated with rotation of the methyl groups and these are due to the constraints imposed by the symmetry.

Solvation energies based on single-point calculations using THF as solvent were carried out on the optimised HF/3-21G geometries with $C_{5v}$ symmetry. Solvation energies were computed with Jaguar program suite (Version 4.2), using a continuum dielectric solvent approach. Calculated solvation energies in kcal mol$^{-1}$ of **2**·X$^-$ (X = Cl$^-$, Br$^-$, I$^-$) with $C_{5v}$ symmetry (HF/3-21G geometries); Cl −38.94, Br −34.50, I −33.65. Thus no important effects of solvation on the complex stabilities were observed and the trend in energy when considering solvation is the same as in the gas-phase calculations, that is, Cl > Br > I.

## Acknowledgement

We gratefully acknowledge the EPSRC (F.G., M.McP., D.S.W.), the EU (Fellowship for L.R., Erasmus studentship I.K.), The States of Guernsey and The Domestic and Millennium Fund (R.A.K.), Unilever (M.A.S.), St. Catharine's College Cambridge (Fellowship for A.D.W.) and The Cambridge European Trust (F.G.) for financial support. We also thank Prof. J. K. M. Sanders for valuable discussions and Dr. J. Davies for collecting X-ray data on **2**·HBr·THF and **2**·I{Li(thf)$_4$}.

[1] O. J. Scherer, K. Andres, C. Krüger, Y.-H. Tsay, G. Wolmerhäuser, *Angew. Chem.* **1980**, *92*, 563; *Angew. Chem. Int. Ed. Engl.* **1980**, *19*, 571; J. K. Brask, T. Chivers, M. L. Krahn, M. Parvez, *Inorg. Chem.* **1999**, *38*, 290.

[2] M. L. Thompson, A. Tarassoli, R. C. Haltiwanger, A. D. Norman, *Inorg. Chem.* **1987**, *26*, 684.

[3] A. Bashall, E. L. Doyle, C. Tubb, S. J. Kidd, M. McPartlin, A. D. Wood, D. S. Wright, *Chem. Commun.* **2001**, 2542.

[4] A. Bashall, A. D. Bond, E. L. Doyle, F. García, S. Kidd, G. T. Lawson, M. McPartlin, M. C. Parry, A. D. Woods, D. S. Wright, *Chem. Eur. J.* **2002**, *8*, 3377.

[5] E. Niecke, D. Gudat, E. Symalla, *Angew. Chem.* **1986**, *98*, 817; *Angew. Chem. Int. Ed. Engl.* **1986**, *25*, 834.

[6] J. E. Huheey, E. A. Keiter, R. L. Keiter, *Inorganic Chemistry*, 4th ed., Cummings, San Francisco, **1997**, p. 292, and references therein.

[7] W. J. Hehre, L. Radom, P. von R. Schleyer, J. A. Pople, *Ab Initio Molecular Orbital Theory*, Wiley, New York, **1986**.

[8] Optimisation calculations were carried out using GAMESS version 6/20/2002: M. W. Schmidt, K. K. Baldridge, J. A. Boatz, S. T. Elbert, M. S. Gordon, J. H. Jensen, S. Koseki, N. Matsunaga, K. A. Nguyen, S. J. Su, T. L. Windus, M. Dupuis, J. A. Montgomery, *J. Comput. Chem.* **1993**, *14*, 1347.

[9] a) A. D. Becke, *J. Chem. Phys.* **1993**, *98*, 5648. b) C. Lee, W. Yang, R. Parr, *Phys. Rev. B* **1988**, *37*, 785.

[10] M. C. Thomson, P. H. Busch, *J. Am. Chem. Soc.* **1964**, *86*, 213.

[11] S. Anderson, H. L. Anderson, J. K. M. Sanders, *Acc. Chem. Res.* **1993**, *26*, 469.

[12] S. Anderson, H. L. Anderson, J. K. M. Sanders, *J. Chem. Soc. Perkin Trans. 1* **1995**, 2255.

[13] R. Jefferson, J. F. Nixon, T. M. Painter, R. Keat, L. Stobbs, *J. Chem. Soc. Dalton Trans.* **1973**, 1414.

[14] G. M. Sheldrick, SHELX-97, Göttingen, Germany, **1997**.

Received: March 31, 2004
Published online: October 28, 2004

  